TECHNICAL EVALUATION OF SIEMENS MAMMOMAT INSPIRATION FULL FIELD DIGITAL MAMMOGRAPHY SYSTEM

NHSBSP Equipment Report 0909
December 2009

Authors

KC Young, JM Oduko, O Gundogdu and A Alsager
all of the National Co-ordinating Centre for the Physics of Mammography, Guildford

Enquiries

Enquiries about this report should be addressed to:

Professor KC Young
National Co-ordinating Centre for the Physics of Mammography
Medical Physics Department
Royal Surrey County Hospital
Guildford
GU2 7XX

Tel: 01483 406738
Fax: 01483 406742
Email: ken.young@nhs.net

Published by

NHS Cancer Screening Programmes
Fulwood House
Old Fulwood Road
Sheffield
S10 3TH

Tel: 0114 271 1060
Fax: 0114 271 1089
Email: info@cancerscreening.nhs.uk
Website: www.cancerscreening.nhs.uk

Typeset by Prepress Projects Ltd, Perth (www.prepress-projects.co.uk)
Printed by Henry Ling Limited

CONTENTS

ACKNOWLEDGEMENTS

The authors are grateful to the staff at King's College University Hospital, London, for their help in evaluating the unit at their site.

1. INTRODUCTION

1.1 Testing procedures and performance standards for digital mammography

This report is one of a series evaluating commercially available digital mammography systems on behalf of the NHS Breast Screening Programme (NHSBSP). The testing methods and standards applied are mainly derived from NHSBSP Equipment Report 0604.[1] The report is referred to in this document as the NHSBSP protocol and it uses the same image quality and dose standards as those provided in the European protocol.[2,3] The European protocol was followed where there is a more detailed performance standard, eg for the automatic exposure control (AEC) system.

1.2 Objectives

The purpose of these tests was to determine whether this system meets the main standards in the NHSBSP and European protocols and to provide performance data for comparison against other manufacturers' products. Additional measurements were also undertaken to assess how well the system's AEC was optimised. The method for assessing optimisation has been reported previously.[4,5] Clinical evaluations are published separately by the NHSBSP where systems meet the minimum standards in the NHSBSP protocol. A final decision on the suitability of systems for use in the NHSBSP depends on a review of both the technical and the clinical evaluation.

2. METHODS

2.1 System tested

The tests were conducted at the King's College Hospital, London, on the Siemens Mammomat Inspiration Full Field Digital Mammography (FFDM) system shown in Figure 1 and described in Table 1. The AEC can be set to provide a reduced dose that is approximately 20% lower than in the standard dose mode. The 'segmentation' option searches for the area of densest breast tissue. An explanation of how the AEC is designed to work is supplied in section 9. (Note that the older design of AEC software discussed in section 9 was in use when these tests were conducted.)

Figure 1 Photograph of Siemens Mammomat Inspiration FFDM system.

Table 1 System description

Target materials	Molybdenum and tungsten
Added filtration	30 µm molybdenum 25 µm rhodium with Mo tube 50 µm rhodium with W tube
Pixel size	85 µm (in detector plane)
Detector area	24 × 30cm
Pixel array	2816 × 3584
Focus to image receiver	650.0 mm (Mo target) 655.5 mm (W target)
AEC modes	Opdose*, AEC segmentation on or off, low dose mode with AEC segmentation on or off
Software version	VB10D (125P01)
Detector serial number	Detector LMAM – serial number 163

*System that suggests automatic exposure parameters to match the thickness of the breast.

2.2 Detector response

The detector response was measured broadly as described in the NHSBSP protocol. A phantom of Plexiglas (polymethylmethacrylate, or PMMA) with a total thickness of 45 mm was placed at the tube exit port and exposed using the three target/filter combinations available (Mo/Mo, Mo/Rh and W/Rh) at tube voltages spanning the range used clinically (25, 28, 31 and 34 kV). An ion chamber was positioned at the surface of the breast support table, and the entrance surface air kerma measured for a single tube current–time product for each tube voltage and target/filter combination tested. The readings were corrected to the surface of the imaging detector using the inverse square law. It was established that the imaging detector is at a distance of 650 mm from the tube focus and 17 mm below the protective cover. No correction was made for attenuation by the protective plates above the detector but the grid was removed. The images were saved as unprocessed files and transferred to another computer for analysis. A 10 mm square region of interest (ROI) was positioned on the midline and 6 cm from the chest wall edge of each image. The average pixel value and the standard deviation of pixel values within that region were measured. The relationship between average pixel values and the detector entrance surface air kerma was determined, as was the magnitude of the pixel offset at zero air kerma.

2.3 Dose measurement

Doses were measured by using the AEC in each of its different modes (AEC segmentation on or off, low dose setting applied or not applied) to expose different thicknesses of PMMA each with an area of 18 × 24 cm. Small PMMA spacers were added at the edge of the test object to adjust the total thickness to the equivalent breast thickness. Mean glandular doses (MGDs) were calculated for the equivalent breast thicknesses and the displayed doses recorded. To measure the contrast-to-noise ratio (CNR) an aluminium square, 10 × 10 mm and 0.2 mm thick, was placed on top of a 20 mm thick block, with one edge on the midline and 6 cm from the chest wall edge. Additional layers of PMMA were placed on top to vary the total thickness.

2.4 Contrast-to-noise ratio

The images of the blocks of PMMA obtained during the dose measurement were analysed to obtain the CNRs. Twenty small square ROIs (approximately 2.5 × 2.5 mm) were used to determine the average signal and the standard deviations in the signal within the image of the aluminium square (four ROIs) and the surrounding background (16 ROIs) as shown in Figure 2. Small ROIs are used to minimise distortions produced by the heel effect. However that is less important for this system because flat field correction is applied. The CNR was calculated for each image as defined in the NHSBSP and European protocols.

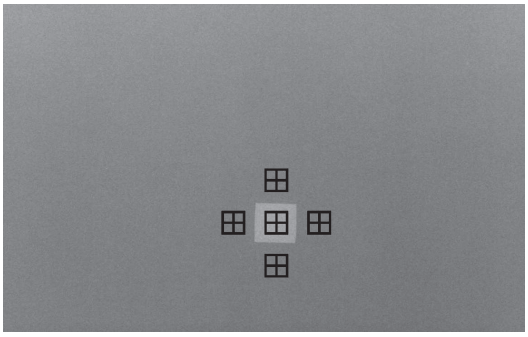

Figure 2 Location and size of ROIs used to determine the CNR.

To apply the standards in the European protocol the limiting value for CNR (using 50 mm PMMA) was determined according to equation 1. This determines the CNR value ($CNR_{limiting\ value}$) needed to achieve the minimum threshold gold thickness for the 0.1 mm detail (ie $threshold\ gold_{limiting\ value} = 1.68$ µm which is equivalent to $threshold\ contrast_{limiting\ value} = 23.0\%$ using 28 kV Mo/Mo). Threshold contrasts were calculated as described in the European protocol and used in equation 1.

$$CNR_{limiting\ value} = CNR_{measured} \times \frac{TC_{measured}}{TC_{limiting\ value}} \quad (1)$$

The relative CNR was then calculated according to equation 2 and compared with the limiting values provided for relative CNR shown in Table 2. The minimum CNR required to meet this criterion was then calculated.

$$Relative\ CNR = CNR_{measured}/CNR_{limiting\ value} \quad (2)$$

Table 2 Limiting values for relative CNR

Thickness of PMMA (mm)	Equivalent breast thickness (mm)	Limiting values for relative CNR (%) in European protocol
20	21	>115
30	32	>110
40	45	>105
45	53	>103
50	60	>100
60	75	>95
70	90	>90

2.5 AEC performance for local dense areas

The method used in the European type testing protocol was followed. To simulate local dense areas nine images were made with different thicknesses (2–18 mm) of extra attenuation added, so that the compression plate remained in position at 40 mm height, as shown in Figure 3.

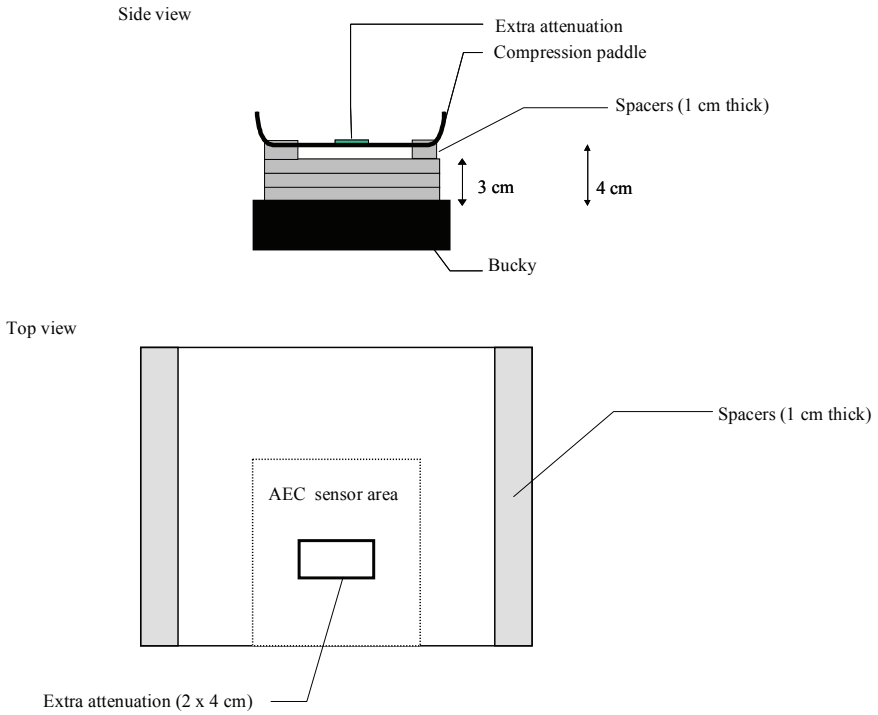

Figure 3 Set-up to measure AEC performance for local dense areas.

In the area of the extra attenuation (20 × 40 mm PMMA) the mean pixel value and standard deviation of a ROI of 2.5 × 2.5 mm were measured and the signal-to-noise ratio (SNR) calculated.

2.6 Noise analysis

The 45 mm thick block of PMMA with aluminium square used for the measurement of CNR was exposed using manually selected tube loading across the range available. The kV target/filter combination used was that selected by the AEC for 45 mm PMMA. The compression paddle was in place. The same ROIs used in the CNR measurement were applied to the corresponding unprocessed images. The average standard deviations of the pixel values in the background ROI for each image were used to investigate the relationship between dose to the detector and image noise. It was assumed that this noise comprises three components, electronic noise, structural noise and quantum noise, with the relationship shown in equation 3. This method of analysis has been described previously.[5]

$$\sigma_p = \sqrt{k_e^2 + k_q^2 p + k_s^2 p^2} \quad (3)$$

where σ_p is the standard deviation in pixel values within an ROI with a uniform exposure and a mean pixel value p, and k_e, k_q and k_s are the coefficients determining the amount of electronic, quantum and structural noise in a pixel with a value p. For simplicity the noise is sometimes presented here as relative noise defined as in equation 4.

$$\textit{Relative noise} = \frac{\sigma_p}{p} \quad (4)$$

The variation in relative noise with mean pixel value was evaluated and fitted using equation 3; non-linear regression was used to determine the best fit for the constants and their asymptotic confidence limits (using Graphpad Prism Version 5.00 for Windows, Graphpad software, San Diego, CA, USA, www.graphpad.com). This established whether the experimental measurements of the noise fitted this equation, and the relative proportions of the different noise components. In fact the relationship between noise and pixel values has been found empirically to be approximated by a simple power relationship as shown in equation 5.

$$\frac{\sigma_p}{p} = k_t p^{-n} \quad (5)$$

where k_t is a constant. If the noise were purely quantum noise the value of n would be 0.5. However the presence of electronic and structural noise means that n can be slightly higher or lower than 0.5.

2.7 Image quality measurements

Contrast–detail measurements were made using the CDMAM phantom (version 3.4, UMC St. Radboud, Nijmegen University, the Netherlands). The phantom was positioned with a 20 mm thickness of PMMA above and below, to give a total attenuation approximately equivalent to 50 mm of PMMA or 60 mm thickness of typical breast tissue. This arrangement was imaged using the x-ray set's AEC with small PMMA spacers at the edges to create a total thickness of 60 mm. The nearest manually selected mAs to the AEC-selected value was then used to image the phantom, with this value subsequently referred to as that which gave 'normal dose'. The exposure was repeated, with small adjustments to the phantom position, to obtain a representative sample of 16 images at this dose level. Unprocessed images were transferred to disk for subsequent analysis off-site. Further images of the test phantom were then obtained at other dose levels by manually selecting higher and lower mAs values with the same beam quality.

An automatic method of reading the CDMAM images was used.[6–8] The threshold gold thickness for a typical human observer was predicted using equation 6.

$$TC_{predicted} = rTC_{auto} \quad (6)$$

where $TC_{predicted}$ is the predicted threshold contrast for a typical observer and TC_{auto} is the threshold contrast measured using an automated procedure with CDMAM images. Contrasts were calculated from gold thickness for a nominal tube voltage of 28 kV and a Mo/Mo target/filter combination as described in the European protocol. r is the average ratio between human and automatic threshold contrast determined experimentally with the values shown in Table 3.[6]

Table 3 Values of *r* used to predict threshold contrast

Diameter of gold disc (mm)	Average ratio of human to automatically measured threshold contrast (*r*)
0.08	1.40
0.10	1.50
0.13	1.60
0.16	1.68
0.20	1.75
0.25	1.82
0.31	1.88
0.40	1.94
0.50	1.98
0.63	2.01
0.80	2.06
1.00	2.11

The main advantage of automatic reading is that it has the potential to eliminate observer error, which is a significant problem when using human observers. However it should be noted that the official protocols are presently based on human reading.

The predicted threshold gold thickness for each detail diameter at each dose level was fitted with a curve as described in the NHSBSP protocol. The confidence limits for the predicted threshold gold thicknesses have been previously determined by a resampling method using a large set of images. The threshold contrasts quoted in the tables of results are derived from the fitted curves, as this has been found to improve accuracy.[6]

The expected relationship between threshold contrast and dose is shown in equation 7.

$$Threshold\ contrast = \lambda D^{-n} \quad (7)$$

D represents the MGD for a 60 mm thick standard breast equivalent to the test phantom configuration used for the image quality measurement. λ is a constant to be fitted. It is assumed that a similar equation applies when using threshold gold thickness instead of contrast. This equation was plotted with the experimental data for each detail size from 0.1 to 1.0 mm. The value of *n* with the best fit to the experimental data was determined.

Human readings of the CDMAM images were also obtained. This was done by averaging the results from 12 readings, with three different readers each reading four images. Curve-fitting as described above was applied to the results.

2.8 Optimisation

A method for determining optimal beam qualities and exposure factors for digital mammography systems (described previously)[4,5] was used to evaluate this system. CNR and MGD were measured as described above using blocks of PMMA from 20 to 70 mm thick. For each thickness four tube voltage settings were used (25, 28, 31 and 34 kV) with each of the target/filter combinations available, and the mAs were recorded. The MGDs to typical breasts with attenuation equivalent to each thickness of the PMMA were calculated as described in the NHSBSP protocol. Each exposure was designed to achieve a standard pixel value. The relationship between noise and pixel values in digital mammography systems has been shown previously[5] to be approximated by

$$\text{Relative noise} = \frac{\sqrt{\frac{sd(bgd)^2 + sd(Al)^2}{2}}}{p} = k_t p^{-n} \quad (8)$$

where k_t is a constant, and p is the average background pixel value linearised with absorbed dose to the detector. *sd(bgd)* is the average standard deviation of pixel values in the ROIs over the background. *sd(Al)* is the average standard deviation of pixel values in an ROI over a $0.2 \times 10 \times 10$ mm piece of aluminium. The value of n was found by fitting this equation to the experimental data. Equation 9 was then used to calculate the dose required to achieve a target CNR, where k is a constant to be fitted and D is the MGD for a breast of equivalent thickness.

$$CNR = kD^n \quad (9)$$

The target CNR was that calculated to reach either the minimum or the achievable image quality in the NHSBSP and European protocols using the following relationship

$$\text{Threshold contrast} = \frac{\lambda}{CNR} \quad (10)$$

where λ is a constant that is independent of dose, beam quality and the thickness of attenuating material. The optimal beam quality for each thickness was selected as that necessary to achieve the target CNR for the minimum dose.

3. RESULTS

3.1 Detector response

The detector was found to have a linear response, with an offset of 50, as shown in Figure 4. The gradient was measured as 0.308 µGy per pixel value at 29 kV W/Rh. The exposures selected by the AEC resulted in average pixel values of approximately 340 using the normal dose mode. A standard value of 340 was chosen to determine the reference entrance air kerma, which was 89.3 µGy using 29 kV W/Rh. The corresponding reference entrance air kermas to produce pixel values of 340 using other beam qualities are shown in Figure 5.

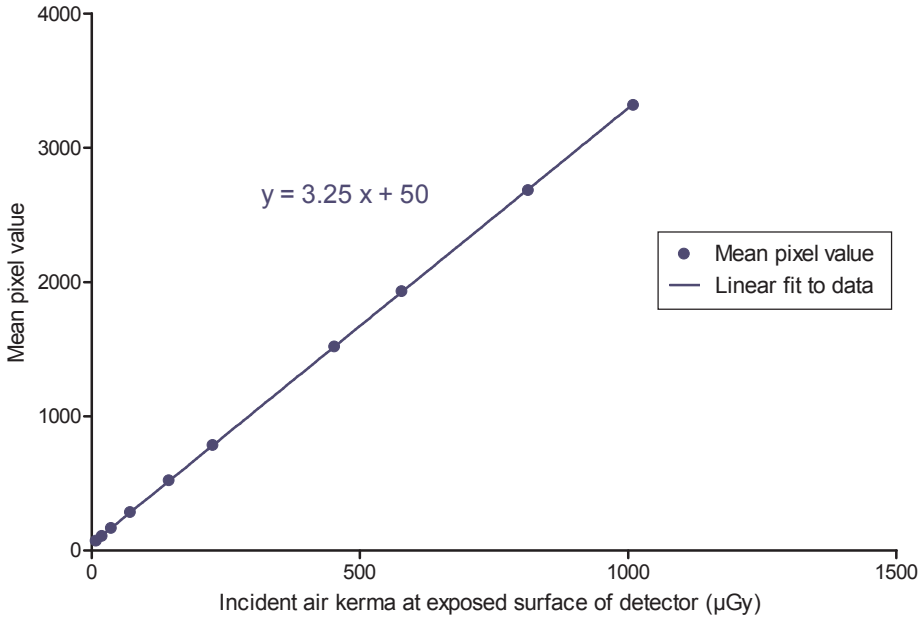

Figure 4 Detector response curve.

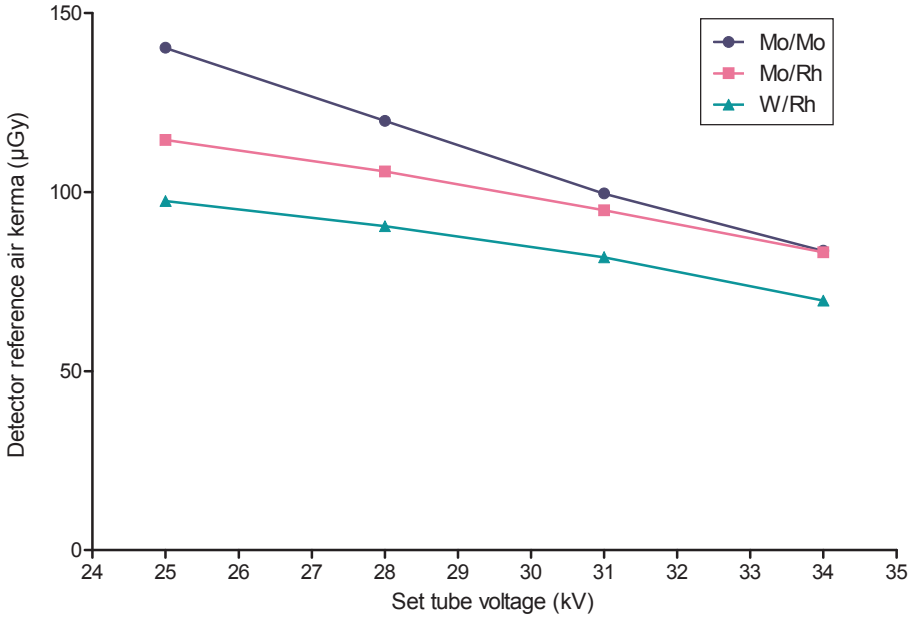

Figure 5 Detector reference air kerma for a pixel value of 340.

3.2 AEC performance

3.2.1 Dose

The MGDs for breasts simulated with PMMA exposed under AEC control are shown in Table 4 and Figure 6. At all thicknesses the dose was below the remedial level in the NHSBSP protocol which is the same as the maximum acceptable level in the European protocol.

Table 4a MGD for simulated breasts (AEC with segmentation on)

PMMA thickness (mm)	Equivalent breast thickness (mm)	kV	Target	Filter	mAs	MGD (mGy)	mAs (low dose mode)	MGD (mGy) (low dose mode)	% decrease with 'low'	NHSBSP remedial level (mGy)
20	21	26	W	Rh	32.7	0.57	27.3	0.48	17	>1.0
30	32	27	W	Rh	48.7	0.76	40.3	0.63	17	>1.5
40	45	28	W	Rh	72.7	1.05	58.8	0.85	19	>2.0
45	53	29	W	Rh	81.0	1.19	66.0	0.97	19	>2.5
50	60	30	W	Rh	91.7	1.37	72.9	1.09	21	>3.0
60	75	31	W	Rh	130.0	1.88	109.6	1.59	16	>4.5
70	90	32	W	Rh	177.8	2.47	140.8	1.96	21	>6.5

Table 4b MGD for simulated breasts (AEC with segmentation off)

PMMA thickness (mm)	Equivalent breast thickness (mm)	kV	Target	Filter	mAs	MGD (mGy)	mAs (low dose mode)	MGD (mGy) (low dose mode)	% decrease with 'low'	NHSBSP remedial level (mGy)
20	21	26	W	Rh	31.2	0.55	26.0	0.45	17	>1.0
30	32	27	W	Rh	46.2	0.72	37.7	0.59	18	>1.5
40	45	28	W	Rh	68.8	1.00	56.0	0.81	19	>2.0
45	53	29	W	Rh	77.0	1.13	62.5	0.92	19	>2.5
50	60	30	W	Rh	84.9	1.27	71.1	1.06	16	>3.0
60	75	31	W	Rh	122.3	1.77	100.8	1.46	18	>4.5
70	90	32	W	Rh	171.7	2.39	133.1	1.85	22	>6.5

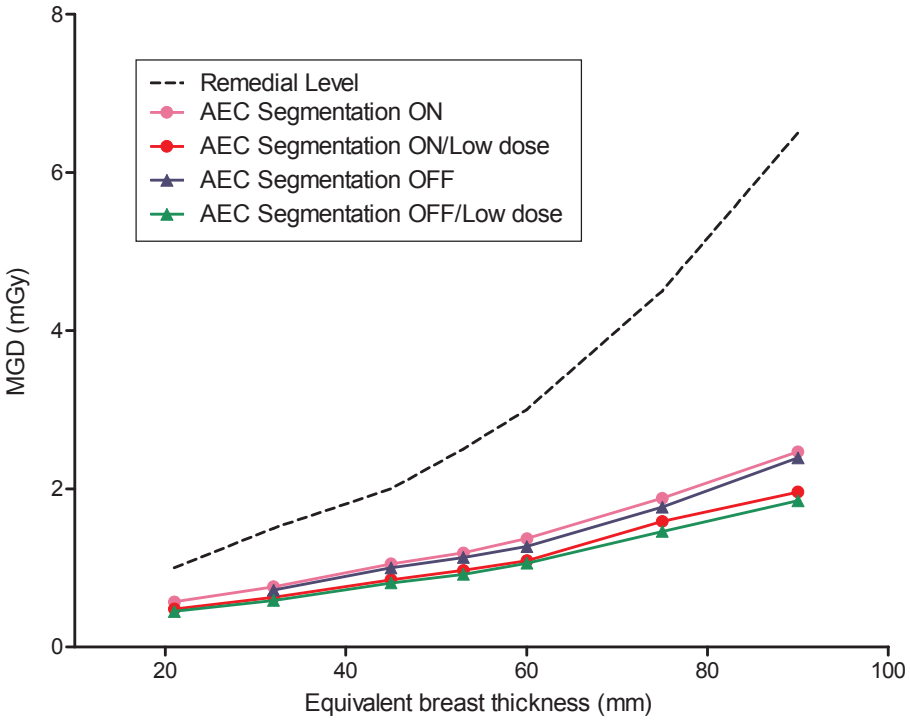

Figure 6 MGD for different thicknesses of simulated breasts in different modes.

3.2.2 CNR

The results of the contrast and CNR measurements are shown in Table 5 and Figure 7. The CNRs required to meet the minimum acceptable and achievable image quality standards at the 60 mm breast thickness have been calculated and are shown in Table 4 and Figure 7. The CNRs required at each thickness to meet the limiting values for CNR in the European protocol are also shown.

Table 5a Contrast and CNR measurements: AEC segmentation on, normal dose

Equivalent breast thickness (mm)	kV target/ filter	mAs	Back-ground pixel value	% contrast for 0.2 mm Al	Measured CNR	CNR at minimum acceptable image quality*	CNR at achievable image quality*	CNR to meet European limiting value	European limiting values for relative CNR
21	26 W/Rh	32.7	376	16.0%	9.8	4.22	6.15	4.86	>115
32	27 W/Rh	48.7	373	14.8%	8.8	4.22	6.15	4.64	>110
45	28 W/Rh	72.7	370	13.8%	8.2	4.22	6.15	4.43	>105
53	29 W/Rh	81	364	13.1%	7.6	4.22	6.15	4.35	>103
60	30 W/Rh	91.7	361	12.4%	7.1	4.22	6.15	4.22	>100
75	31W/Rh	130	362	11.4%	6.3	4.22	6.15	4.01	>95
90	32 W/Rh	177.8	365	10.1%	5.4	4.22	6.15	3.80	>90

*The target CNR values were determined from the automatic measurements on CDMAM images.

Table 5b Contrast and CNR measurements: AEC segmentation on, low dose

Equivalent breast thickness (mm)	kV target/ filter	mAs	Back-ground pixel value	% contrast for 0.2 mm Al	Measured CNR	CNR at minimum acceptable image quality	CNR at achievable image quality	CNR to meet European limiting value	European limiting values for relative CNR
21	26 W/Rh	27.3	312	16.0	8.6	4.22	6.15	4.86	>115
32	27 W/Rh	40.3	313	14.7	7.8	4.22	6.15	4.64	>110
45	28 W/Rh	58.8	306	13.7	7.0	4.22	6.15	4.43	>105
53	29 W/Rh	66	303	13.1	6.6	4.22	6.15	4.35	>103
60	30 W/Rh	72.9	295	12.4	6.0	4.22	6.15	4.22	>100
75	31W/Rh	109.6	310	11.3	5.6	4.22	6.15	4.01	>95
90	32 W/Rh	140.8	296	10.3	4.8	4.22	6.15	3.80	>90

Table 5c Contrast and CNR measurements: AEC segmentation off, normal dose

Equivalent breast thickness (mm)	kV target/ filter	mAs	Back-ground pixel value	% contrast for 0.2 mm Al	Measured CNR	CNR at minimum acceptable image quality	CNR at achievable image quality	CNR to meet European limiting value	European limiting values for relative CNR
21	26 W/Rh	31.2				4.22	6.15	4.86	>115
32	27 W/Rh	46.2	356	14.7	8.6	4.22	6.15	4.64	>110
45	28 W/Rh	68.8	352	13.8	7.9	4.22	6.15	4.43	>105
53	29 W/Rh	77.0	349	13.1	7.4	4.22	6.15	4.35	>103
60	30 W/Rh	84.9	337	12.4	6.7	4.22	6.15	4.22	>100
75	31W/Rh	122.3	344	11.3	6.1	4.22	6.15	4.01	>95
90	32 W/Rh	171.7	352	10.1	5.3	4.22	6.15	3.80	>90

Table 5d Contrast and CNR measurements: AEC segmentation off, low dose

Equivalent breast thickness (mm)	kV target/ filter	mAs	Back-ground pixel value	% contrast for 0.2 mm Al	Measured CNR	CNR at minimum acceptable image quality	CNR at achievable image quality	CNR to meet European limiting value	European limiting values for relative CNR
21	26 W/Rh	26.0	249	15.9	8.2	4.22	6.15	4.86	>115
32	27 W/Rh	37.7	243	14.9	7.4	4.22	6.15	4.64	>110
45	28 W/Rh	56.0	244	13.7	6.8	4.22	6.15	4.43	>105
53	29 W/Rh	62.5	238	13.0	6.3	4.22	6.15	4.35	>103
60	30 W/Rh	71.1	237	12.5	6.0	4.22	6.15	4.22	>100
75	31W/Rh	100.8	241	11.2	5.3	4.22	6.15	4.01	>95
90	32 W/Rh	133.1	232	10.1	4.5	4.22	6.15	3.80	>90

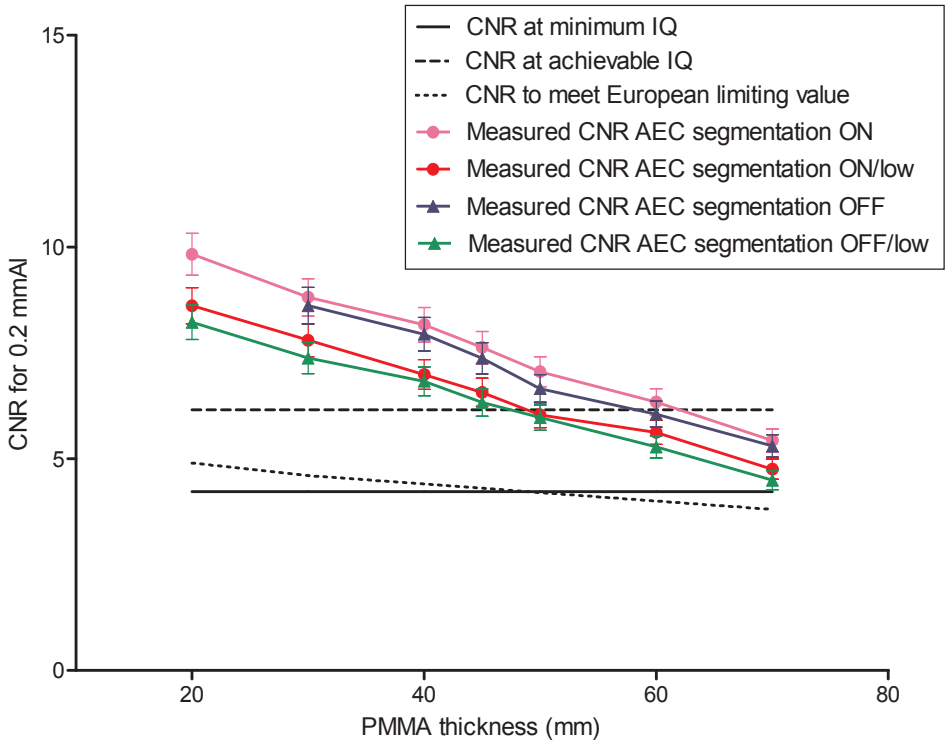

Figure 7 Measured CNR compared with the limiting values in the European protocol for the system. (Error bars indicate 95% confidence limits.)

3.2.3 AEC performance for local dense areas

The results for AEC performance are shown in Table 6 and Figure 8 with segmentation on and off. It is expected that with an AEC that adjusts for locally dense areas the SNR will remain constant with increasing layers of PMMA. In this case the SNR decreased, indicating that the local dense area had no effect on the tube loading, which remained virtually constant.

Table 6a AEC performance for local dense areas: segmentation on

Attenuation (cm PMMA)	Target/filter	Tube voltage (kV)	Tube load (mAs)	SNR
3.0	W/Rh	28	41.9	57.1
3.2	W/Rh	28	42.3	53.1
3.4	W/Rh	28	42.3	49.7
3.6	W/Rh	28	42.0	45.7
3.8	W/Rh	28	42.1	43.0
4.2	W/Rh	28	41.8	36.2
4.6	W/Rh	28	42.3	31.9
4.8	W/Rh	28	42.4	28.9

Table 6b AEC performance for local dense areas: segmentation off

Attenuation (cm PMMA)	Target/filter	Tube voltage (kV)	Tube load (mAs)	SNR
3.0	W/Rh	28	39.7	55.8
3.2	W/Rh	28	39.4	51.2
3.4	W/Rh	28	39.5	47.8
3.6	W/Rh	28	39.4	43.7
3.8	W/Rh	28	42.1	41.0
4.2	W/Rh	28	39.3	35.7
4.6	W/Rh	28	39.8	30.1
4.8	W/Rh	28	39.4	27.7

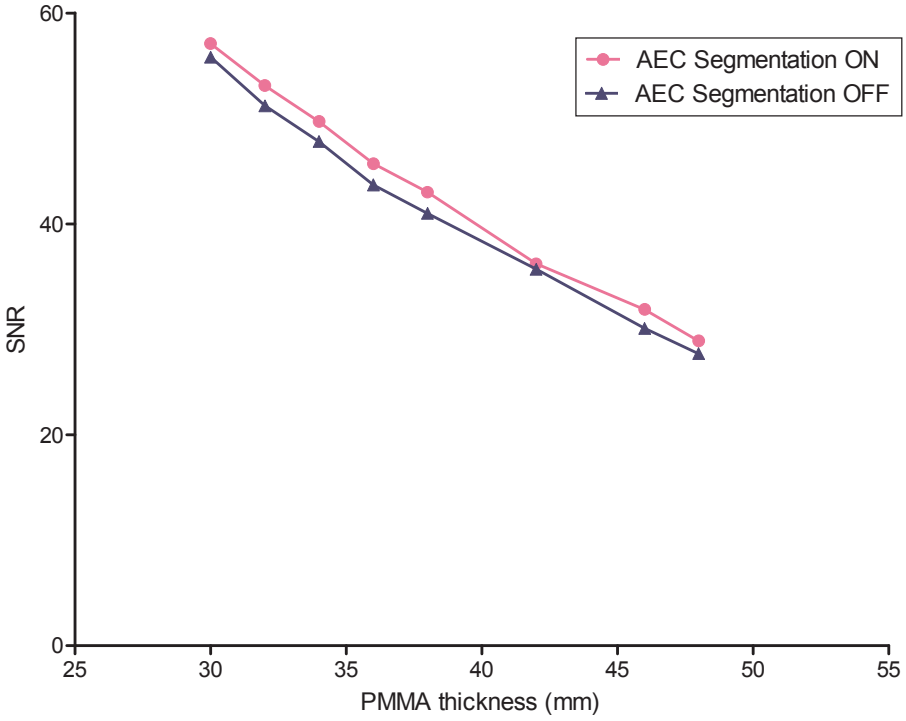

Figure 8 AEC performance for local dense areas.

3.3 Noise measurements

The variation in noise with dose was analysed by plotting the standard deviation in pixel values against the detector entrance air kerma, as shown in Figure 9. The fitted power curve has an index of 0.32. If quantum noise sources alone were present the data would form a straight line with an index of 0.5. The presence of some electronic noise and structural noise has caused the curve to deviate from a straight line. This is normal for such systems and quantum noise was the dominant noise source.

The relative noise is plotted against the background pixel value in Figure 10. The pixel value is proportional to the dose absorbed by the detector. A curve of the form described in equation 5 with an index $n = 0.64$ has been fitted to the measured data. (A value for n of 0.5 would be expected if quantum noise alone were present.)

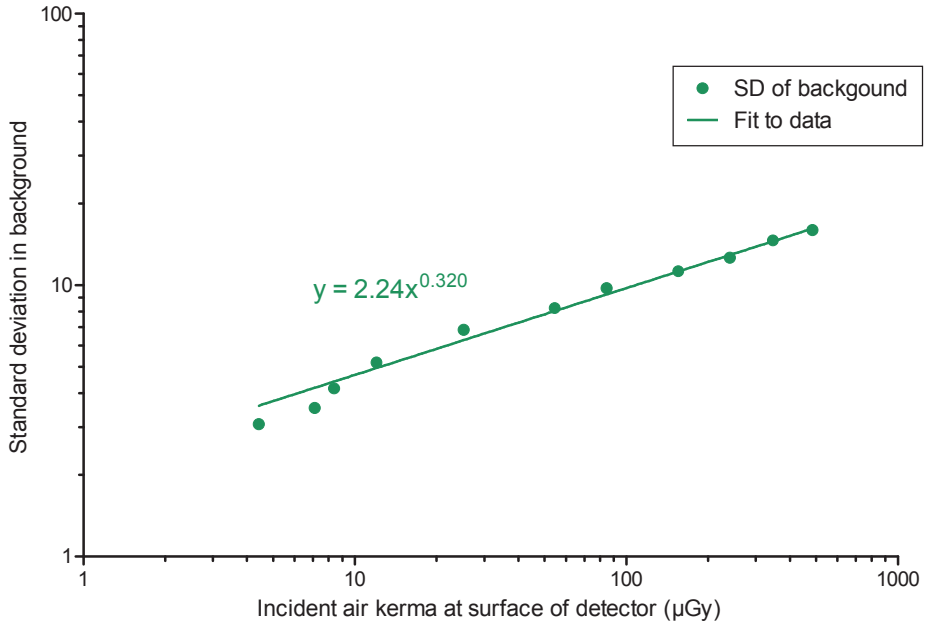

Figure 9 Standard deviation of pixel values versus air kerma at detector.

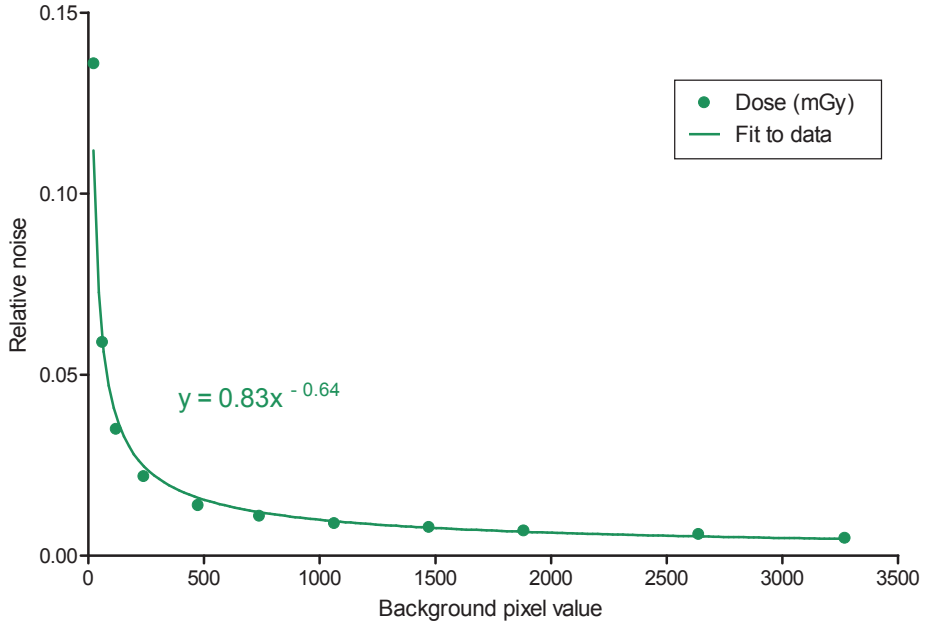

Figure 10 Relative noise at different pixel values.

Figure 11 is an alternative way of presenting the data and shows the relative noise at different average pixel values. The estimated relative contributions of electronic, structural and quantum noise are shown and the quadratic sum of these contributions fitted to the measured noise (using equation 3).

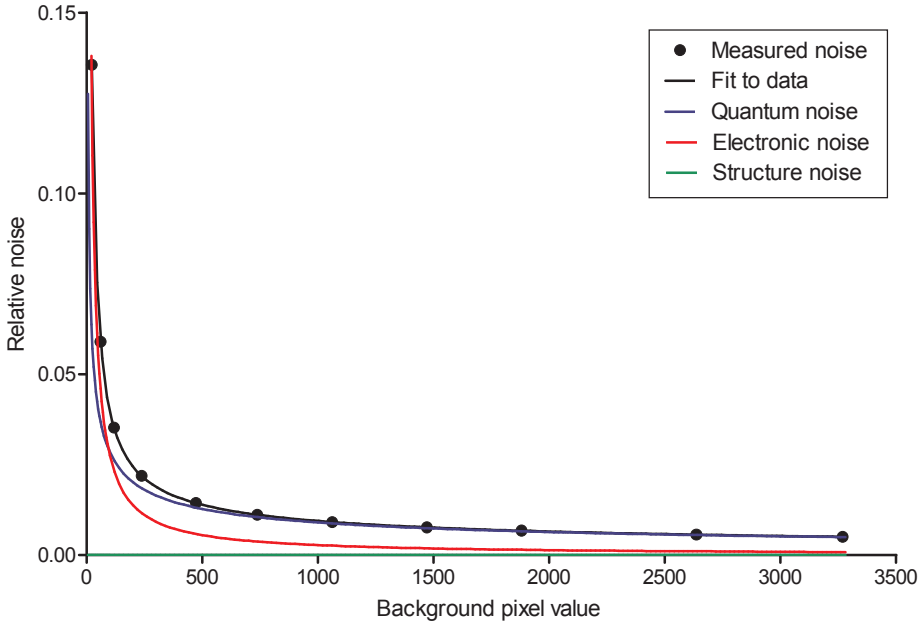

Figure 11 Relative noise and noise components at different pixel values.

3.4 Image quality measurements

The first exposures of the image quality phantom were made using the original Opdose settings to select the beam quality and exposure factors. This resulted in the selection of 28 kV W/Rh and 129.5 mAs and an MGD of 1.38 mGy to an equivalent breast (60 mm thick). (Note that these selections are different from those made after the AEC was adjusted, shown in section 3.2. It was decided not to repeat the image quality measurements at the later settings as the existing measurements already cover a wide range of dose selections.) Subsequent image quality measurements were made at approximately quarter, half, double and quadruple this dose by manual selection of the mAs at the same beam quality as shown in Table 7.

Table 7 Images acquired for image quality measurement

Exposure mode	kV target/filter	Tube loading (mAs)	MGD to equivalent breasts 60 mm thick (mGy)	Number of CDMAM images acquired and analysed
Manual	28 W/Rh	32	0.35	16
Manual	28 W/Rh	63	0.69	16
Manual	28 W/Rh	125	1.38	16
Manual	28 W/Rh	250	2.75	16
Manual	28 W/Rh	450	4.96	16

The contrast–detail curves at the five dose levels are shown in Figure 12. The threshold gold thicknesses for different diameters and the five different dose levels for this system are shown in Table 8, along with the minimum and achievable threshold values from the NHSBSP protocol (which are the same as the European protocol). The data in Table 8 are taken from the fitted curves rather than the raw data.

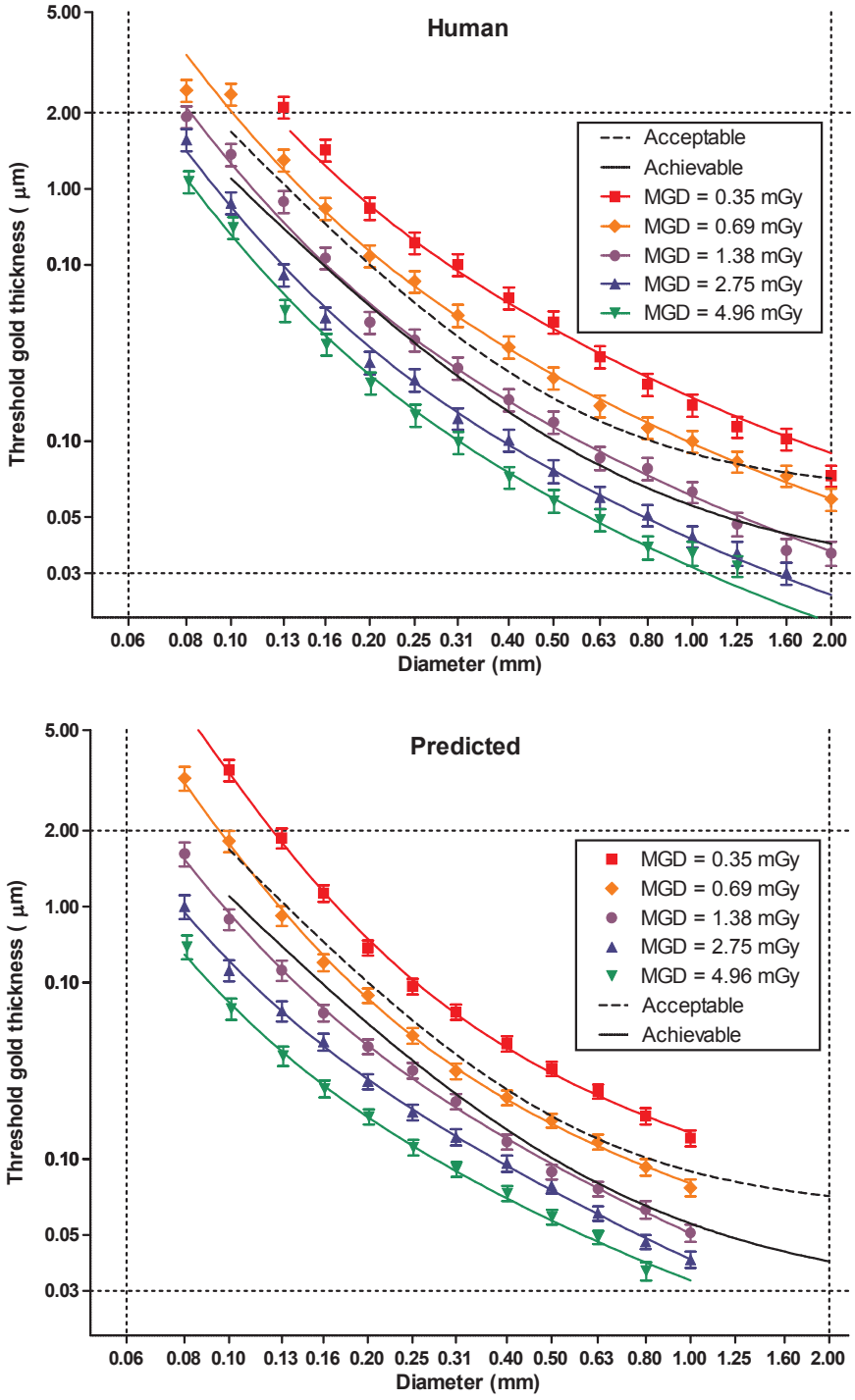

Figure 12 Contrast–detail curves for the system for five different doses at 28 kV W/Rh using human and predicted results from automated reading. The 1.38 mGy dose corresponds to the AEC selection in Opdose mode. (Error bars indicate 95% confidence limits.)

Table 8a Average threshold gold thicknesses for different detail diameters for five different doses using 28 kV W/Rh and human data. (Data are interpolated using curve fits.)

	Threshold gold thickness (µm)						
Diameter (mm)	Acceptable value	Achievable value	MGD = 0.35 mGy	MGD = 0.69 mGy	MGD = 1.38 mGy	MGD = 2.75 mGy	MGD = 4.96 mGy
0.1	1.680	1.100	3.037 ± 0.304	2.059 ± 0.206	1.355 ± 0.136	0.914 ± 0.091	0.674 ± 0.067
0.25	0.352	0.244	0.672 ± 0.067	0.437 ± 0.044	0.260 ± 0.026	0.164 ± 0.016	0.124 ± 0.012
0.5	0.150	0.103	0.284 ± 0.028	0.179 ± 0.018	0.115 ± 0.011	0.075 ± 0.008	0.058 ± 0.006
1	0.091	0.056	0.137 ± 0.014	0.092 ± 0.009	0.060 ± 0.006	0.043 ± 0.004	0.037 ± 0.004

Table 8b Average threshold gold thicknesses for different detail diameters for five different doses using 28 kV W/Rh and predicted data. (Data are interpolated using curve fits.)

	Threshold gold thickness (µm)						
Diameter (mm)	Acceptable value	Achievable value	MGD = 0.35 mGy	MGD = 0.69 mGy	MGD = 1.38 mGy	MGD = 2.75 mGy	MGD = 4.96 mGy
0.1	1.680	1.100	3.337 ± 0.335	1.711 ± 0.172	0.879 ± 0.088	0.563 ± 0.056	0.395 ± 0.040
0.25	0.352	0.244	0.514 ± 0.025	0.308 ± 0.015	0.211 ± 0.010	0.159 ± 0.008	0.114 ± 0.006
0.5	0.150	0.103	0.219 ± 0.012	0.139 ± 0.008	0.095 ± 0.005	0.074 ± 0.004	0.052 ± 0.003
1	0.091	0.056	0.127 ± 0.009	0.079 ± 0.006	0.051 ± 0.004	0.040 ± 0.003	0.029 ± 0.002

In Figure 13, the measured threshold gold thicknesses are plotted against the MGD for an equivalent breast for the 0.1 and 0.25 mm detail sizes. This shows how the threshold gold thickness reduced as the dose was increased. Fitted curves such as those shown in Figure 13 were used to determine the doses needed to meet the minimum acceptable and achievable image quality levels for detail sizes from 0.1 to 1.0 mm; they are shown in Figure 14.

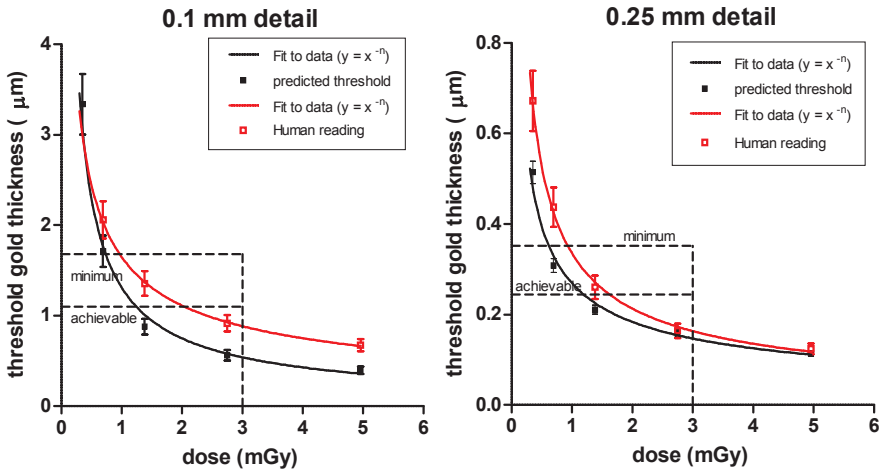

Figure 13 Threshold gold thickness at different doses. (Error bars indicate 95% confidence limits.)

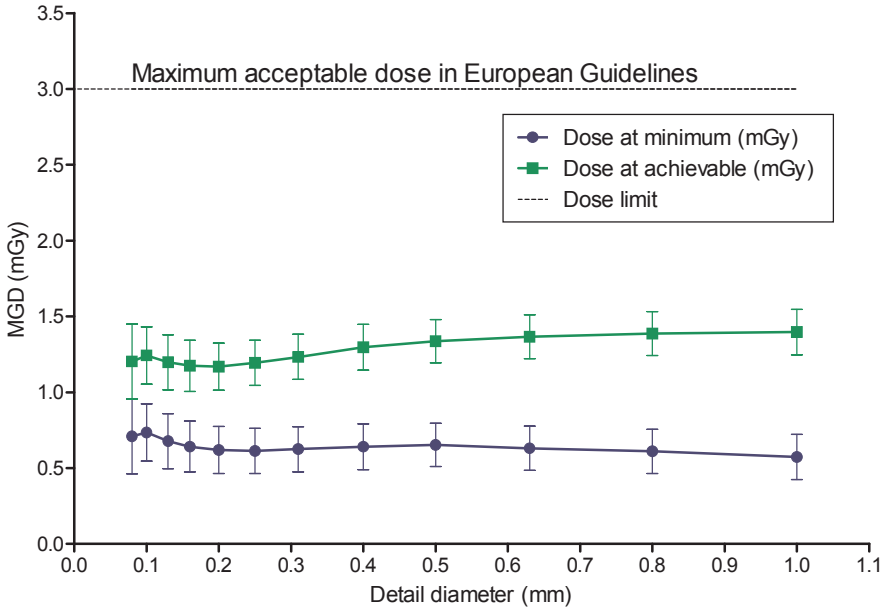

Figure 14 The MGD calculated to be necessary to reach the achievable and minimum acceptable image quality levels at different detail sizes using 28 kV W/Rh for an equivalent breast 60 mm thick. Based on predicted threshold gold thicknesses.

3.5 Comparison with other systems

The MGDs needed to reach the minimum and achievable image quality standards in the NHSBSP protocol have been estimated from the curves shown in Figure 13. (The error in estimating these doses depends on the accuracy of the curve fitting procedure, and pooled data for several systems have been used here to estimate the 95% confidence limits of approximately 20%.) These doses are shown against similar data for other models of digital mammography system in Tables 9 and 10 and Figures 15 to 18. The data for the other systems have been determined in the same way as described in this report and the results published previously.[9–20] The data for film–screens represent an average value determined using a variety of modern film–screen systems.

Table 9 MGD for different systems to reach the minimum threshold gold thickness for 0.1 and 0.25 mm details

	MGD (mGy) for 0.1 mm		MGD (mGy) for 0.25 mm	
System	Human	Predicted	Human	Predicted
Sectra MDM-L30	0.41		0.41	0.42
Siemens Novation*	0.54	0.59	0.47	0.67
Siemens Inspiration	0.97	0.76	0.87	0.60
Hologic Selenia (Mo)	0.85	0.55	0.80	0.53
Hologic Selenia (W)	0.58	0.71	0.65	0.64
GE Essential	0.60	0.49	0.50	0.49
GE DS	1.01	0.82	0.87	0.83
IMS Giotto (W)	1.07	1.38	0.91	1.17
Film–screen	1.17	1.30	1.07	1.36
Fuji Profect CR	1.67	1.78	1.45	1.35
Agfa CR 85-X (MM3.0)†	2.54	2.32	1.45	1.54
Kodak CR (EHR-M2)	2.29	2.34	1.45	1.80
Konica Minolta (CP-1M)	1.60	1.47	1.12	0.99

*Data are the mean of measurements for two systems in NHSBSP Equipment Report 0710.[13]

†Data are the mean of measurements shown in NHSBSP Equipment Reports 0707[12] and 0905.[19]

Table 10 MGD for different systems to reach the achievable threshold gold thickness for 0.1 and 0.25 mm details.

	MGD (mGy) for 0.1 mm		MGD (mGy) for 0.25 mm	
System	Human	Predicted	Human	Predicted
Sectra MDM-L30	1.27	1.74	1.37	0.95
Siemens Novation*	1.30	1.26	1.00	1.37
Siemens Inspiration	2.06	1.27	1.68	1.16
Hologic Selenia (Mo)	1.84	1.19	1.68	1.12
Hologic Selenia (W)	1.66	1.37	1.61	1.48
GE Essential	1.57	1.13	1.14	1.03
GE DS	2.35	1.57	1.80	1.87
IMS Giotto (W)	2.33	2.73	1.77	2.11
Film–screen	2.48	3.03	2.19	2.83
Fuji Profect CR	4.26	3.29	3.52	2.65
Agfa CR 85-X (MM3.0)†	5.21	5.14	3.72	3.82
Kodak CR (EHR-M2)	5.34	5.45	3.03	3.74
Konica Minolta CR (CP-1M)	4.53	3.45	2.73	2.08

*Data are the mean of measurements for two systems in NHSBSP Equipment Report 0710.[13]

†Data are the mean of measurements shown in NHSBSP Equipment Reports 0707[12] and 0905.[19]

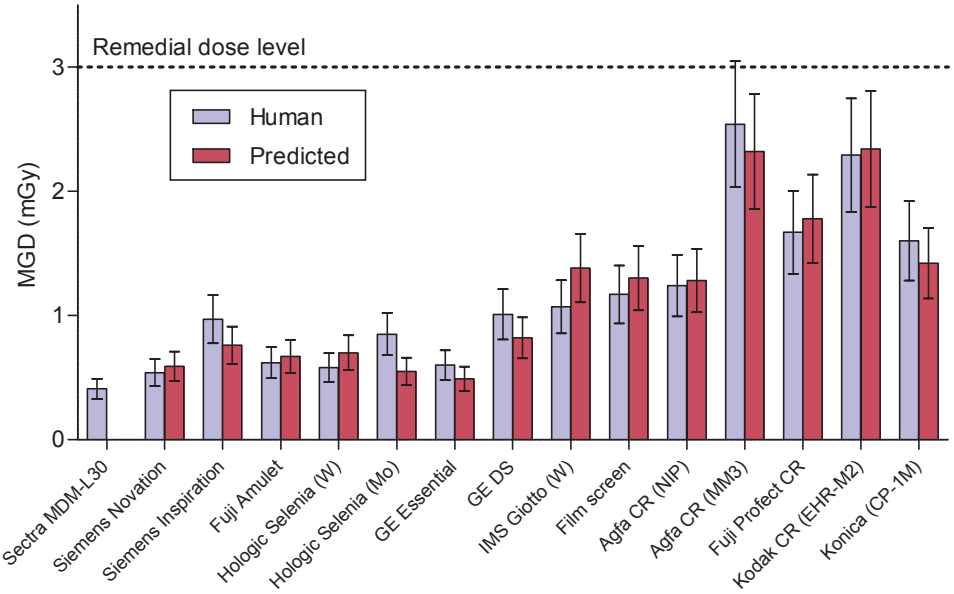

Figure 15 Dose to reach minimum acceptable image quality standard for 0.1 mm detail. (Error bars indicate 95% confidence limits.)

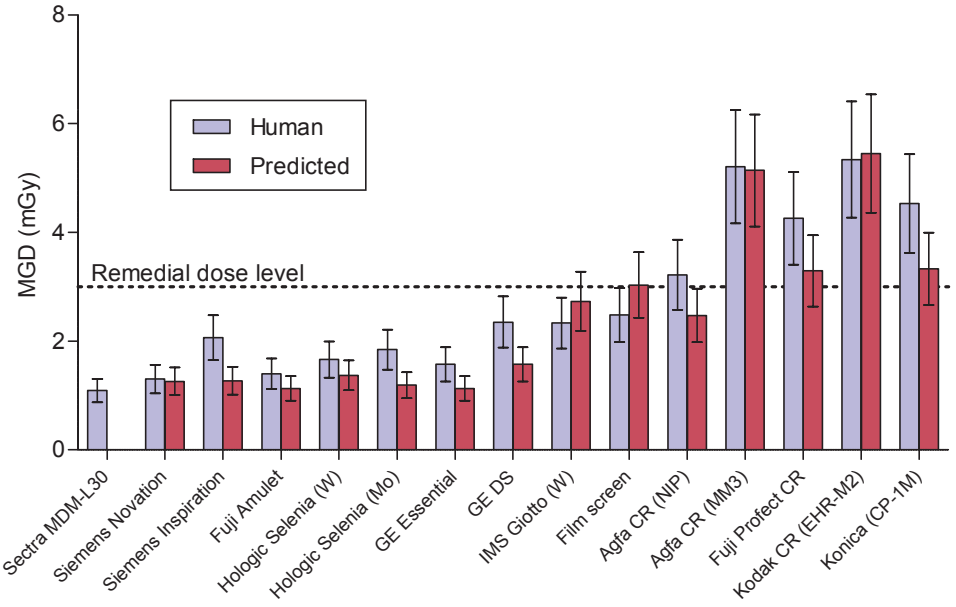

Figure 16 Dose to reach achievable image quality standard for 0.1 mm detail. (Error bars indicate 95% confidence limits.)

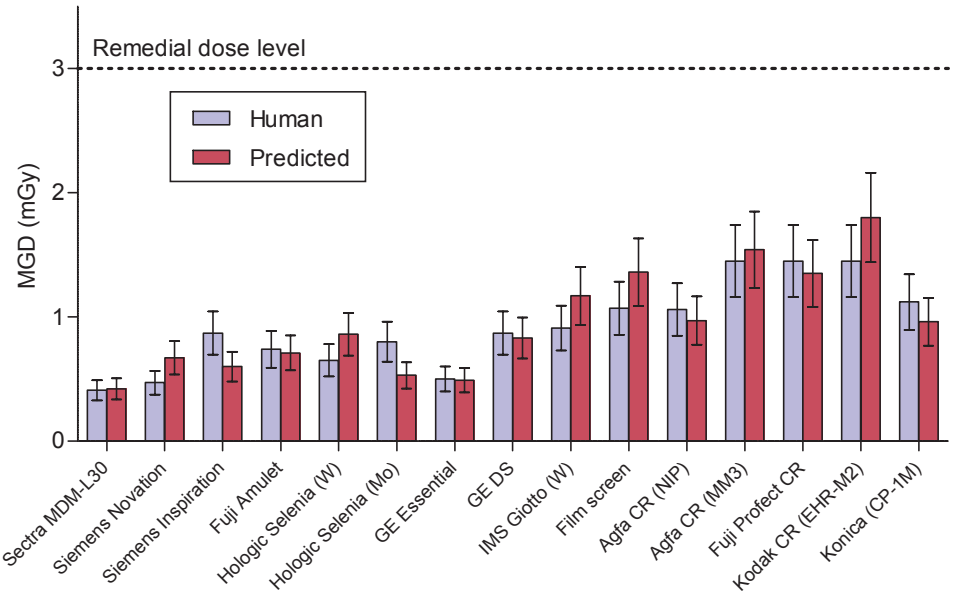

Figure 17 Dose to reach minimum acceptable image quality standard for 0.25 mm detail. (Error bars indicate 95% confidence limits.)

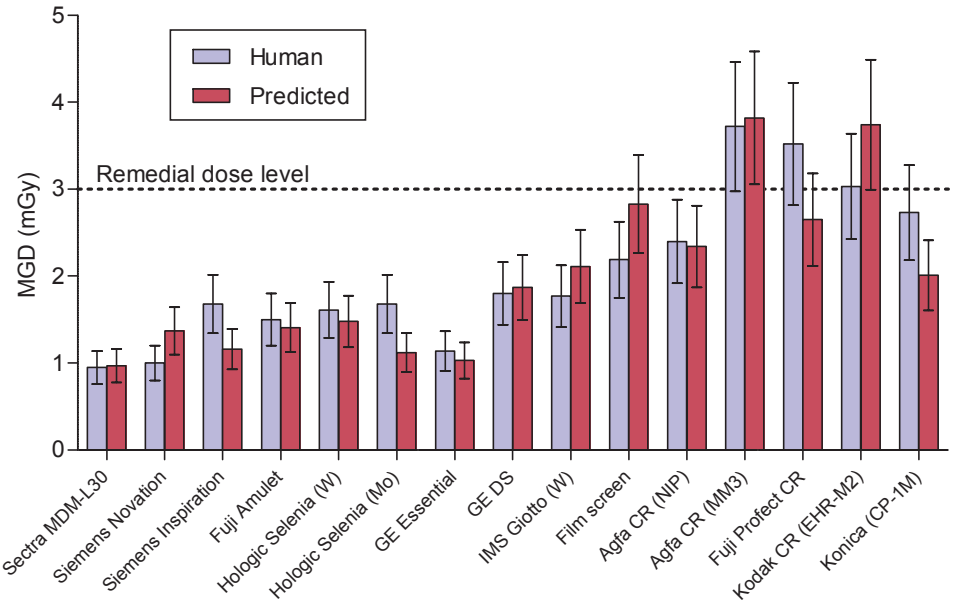

Figure 18 Dose to reach achievable image quality standard for 0.25 mm detail. (Error bars indicate 95% confidence limits.)

3.6 Optimisation

The target CNR corresponding to the achievable image quality standard was calculated to be 6.15. The MGDs needed to reach this target CNR for each beam quality and thicknesses of PMMA are shown in Figure 19. From these data the optimal beam qualities and mAs were calculated and are shown in Table 11.

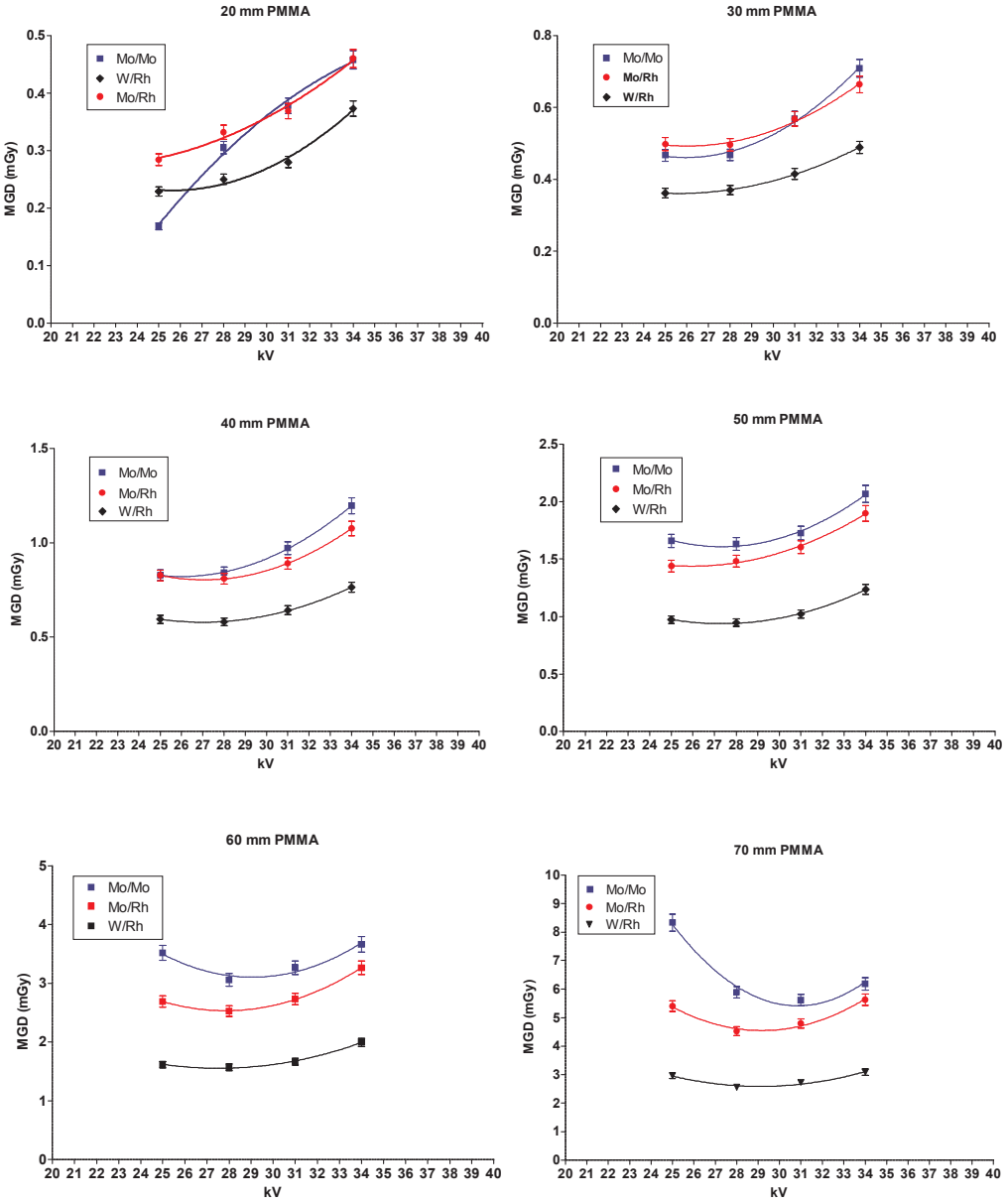

Figure 19 MGD to reach the achievable image quality standard in the NHSBSP protocol (ie CNR = 6.15). (Error bars indicate 95% confidence limits.)

Table 11 Optimal factors to reach achievable image quality (ie where CNR=6.15) at the lowest dose

PMMA thickness (mm)	kV target/filter	Background pixel value	mAs	MGD (mGy)	Remedial dose level in NHSBSP protocol (mGy)
20	25 W/Rh	185	17	0.23	1.0
30	25 W/Rh	204	34	0.36	1.5
40	28 W/Rh	240	45	0.58	2.0
45	28 W/Rh	252	64	0.76	2.5
50	28 W/Rh	259	86	0.95	3.0
60	28 W/Rh	283	163	1.57	4.5
70	28 W/Rh	302	303	2.56	6.5

4. DISCUSSION

The detector response was linear, as expected, with a pixel value offset of 50. The noise analysis confirmed that quantum noise is the dominant noise source. As with most systems there was also evidence of some electronic and structural noise. In all dose modes the AEC produced doses to simulated breasts that were well below the limits in the NHSBSP protocol. The doses for the standard breast simulated with 45 mm of PMMA in the different modes were 0.99 mGy for Opdose (June 2008). They were 1.19 and 1.13 mGy respectively for AEC modes with segmentation on and off (December 2008), and 19% lower for the 'low dose' modes (0.97 and 0.92 mGy respectively). At this thickness an upper limit of 2.5 mGy is applied by the NHSBSP. The doses calculated and displayed by the system itself were different from those calculated by us. The reason for these differences is not clear.

The different AEC modes resulted in relatively constant background pixel values that varied between 335 and 360, and the W/Rh target/filter combination was always selected. This is consistent with the manufacturer's stated aim of maintaining average pixel values within ±15%. The net result of these choices was that the CNR values were relatively high for thinner breasts but dropped steeply with increasing breast thickness. All the AEC modes exceeded the minimum requirements in the European protocol. However the CNR values seemed much higher than necessary for the thinner breasts, while falling below that necessary to reach the achievable level of image quality for the largest simulated thicknesses. At all settings the minimum acceptable CNR value was met or exceeded.

A new test investigated whether the AEC increased exposure when a local area of dense tissue was added. The signal-to-noise ratio in the area of dense tissue decreased with increasing attenuation material, showing that the presence of local density had not modified the exposure. These results indicate that the small area (20 × 40 mm) of simulated dense tissue was not detected by the AEC with the segmentation option. It remains unclear whether larger areas of dense tissue would have triggered an increase in exposure. This is something that could be investigated with reference to clinical images.

The image quality measurements indicated that for the standard thickness tested (equivalent to 50 mm thickness of PMMA, or 60 mm of typical breast) the image quality was close to the achievable level in standard Opdose mode. In this mode the AEC selected a dose of 1.38 mGy using 28 kV W/Rh. Calculations suggested that a dose of approximately 0.8 ± 0.16 mGy was necessary to reach the minimum image quality level for this equivalent breast thickness. A dose of about 1.3 ± 0.3 mGy was calculated to be necessary to reach the achievable image quality level for this equivalent breast thickness.

The doses needed to reach the acceptable and achievable image quality levels are broadly similar to the other DR systems and lower than for film–screen and CR systems.

The optimisation study demonstrated that the use of a W/Rh target/filter combination was optimal across all simulated breast thicknesses. The choice of kV had only a minor effect and the use of slightly higher kV is appropriate for thicker breasts to minimise exposure times. The critical choice is to use a dose large enough to ensure that detector noise is not a limiting factor. For this reason it is suggested that the system be used in standard dose rather than low dose mode. This is likely to be most important for areas of dense tissue with greater breast thicknesses where SNR and CNR values are lowest.

5. CONCLUSIONS

This system is capable of producing excellent image quality for a relatively low radiation dose. As currently set up the AEC will be satisfactory for most types of breast in the different AEC modes. The higher dose mode is recommended. The system met the main standards for dose and image quality in the NHSBSP and European protocols.

6. COMMENTS FROM THE MANUFACTURER ON AEC DESIGN

The original AEC segmentation tested in this report detected almost all of the breast, both dense and non-dense areas, as shown in Figure 20. In this case the AEC would calculate the mAs (and thus the dose) based on the average pixel value received in the prepulse for this region. The average value of the region would lie between the average value of the dense part and the non-dense part of the breast. As a result the average overall value would be higher than the average value in the dense part of the breast alone. The AEC is designed and configured to give the optimal SNR for the calculated average pixel value in the AEC region (the region in Figures 20 and 21 that lies within the green border). An area which has a lower pixel value will therefore produce a lower SNR. This also reduces the CNR. For breasts of the type shown this would result in a final image with a lower SNR and CNR in the dense region, which would contain more noise. As calcifications are small objects which may in some cases resemble noise it was decided to improve the AEC segmentation. Where a breast has both dense and non-dense areas the calculation needs to be based on the densest part of the breast.

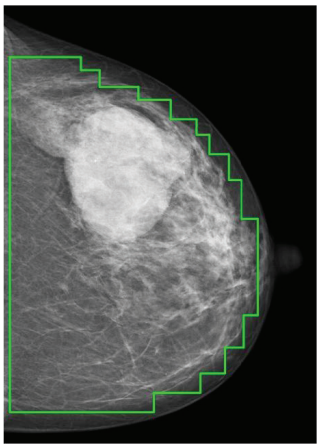

Figure 20 Original AEC segmentation algorithm. Segmented area consists of non-dense and dense parts of the breast.

This modification of the AEC segmentation algorithm involved introducing a second algorithm which segments out the dense part of the breast. When applied to the breast in Figure 20, this new segmentation algorithm would detect the region shown in Figure 21.

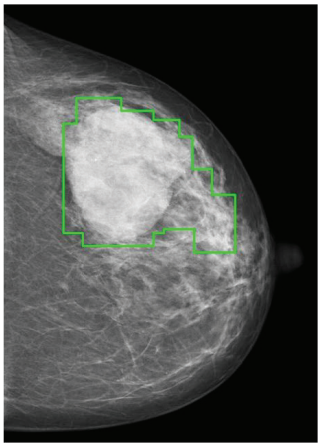

Figure 21 New AEC segmentation algorithm. Segmented area consists of dense part of breast.

REFERENCES

1. Workman A, Castellano I, Kulama E, Lawinski CP, Marshall N, Young KC. *Commissioning and Routine Testing of Full Field Digital Mammography Systems,* 2nd edn. NHS Cancer Screening Programmes, 2006 (NHSBSP Equipment Report 0604).
2. Young KC, Johnson B, Bosmans H, Van Engen R. Development of minimum standards for image quality and dose in digital mammography. In: *Digital Mammography*, *Proceedings of the 7th International Workshop on Digital Mammography*, Durham NC, USA, June 2004 (2005).
3. Van Engen R, Young KC, Bosmans H, Thijssen M. The European protocol for the quality control of the physical and technical aspects of mammography screening. In: *European Guidelines for Breast Cancer Screening,* 4th edn. Luxembourg: European Commission, 2006: 732–739.
4. Young KC, Cook JJH, Oduko JM. Use of the European protocol to optimise a digital mammography system. In: Astley SM, Bradey M, Rose C, Zwiggelaar R, eds. Proceedings of the 8th International Workshop on Digital Mammography. *Lecture Notes in Computer Science*, 2006, 4046: 362–369.
5. Young KC, Oduko JM, Bosmans H, Nijs K, Martinez L. Optimal beam quality selection in digital mammography. *British Journal of Radiology*, 2006, 79: 981–990.
6. Young KC, Cook JJH, Oduko JM, Bosmans H. Comparison of software and human observers in reading images of the CDMAM test object to assess digital mammography systems. In: *Proceedings of SPIE Medical Imaging*, 2006, 614206: 1–13.
7. Young KC, Cook JJH, Oduko JM. Automated and human determination of threshold contrast for digital mammography systems. In: Astley SM, Bradey M, Rose C, Zwiggelaar R, eds. Proceedings of the 8th International Workshop on Digital Mammography*. Lecture Notes in Computer Science*, 2006, 4046: 266–272.
8. Young KC, Alsager A, Oduko JM, Bosmans H, Verbrugge B, Geertse T, Van Engen R. Evaluation of software for reading images of the CDMAM test object to assess digital mammography systems. *Proceedings of SPIE Medical Imaging*, 2008, 69131C, 1–11.
9. Young KC, Oduko JM. *Evaluation of Kodak DirectView Mammography Computerised Radiography.* NHS Cancer Screening Programmes, 2005 (NHSBSP Equipment Report 0504).
10. Young KC, Oduko JM, Woolley L. *Technical Evaluation of the Hologic Selenia Full Field Digital Mammography System.* NHS Cancer Screening Programmes, 2007 (NHSBSP Equipment Report 0701).
11. Young KC, Oduko JM. *Technical Evaluation of the Kodak DirectView Mammography Computerised Radiography System using EHR-M2 Plates.* NHS Cancer Screening Programmes, 2007 (NHSBSP Equipment Report 0706).
12. Young KC, Oduko JM. *Technical Evaluation of the Agfa CR-85 Mammography System.* NHS Cancer Screening Programmes, 2007 (NHSBSP Equipment Report 0707).
13. Young KC, Oduko JM. *Technical Evaluation of the Siemens Novation Full Field Digital Mammography System.* NHS Cancer Screening Programmes, 2007 (NHSBSP Equipment Report 0710).
14. Young KC, Oduko JM. *Technical Evaluation of the Hologic Selenia Full Field Digital Mammography System with a Tungsten Tube.* NHS Cancer Screening Programmes, 2008 (NHSBSP Equipment Report 0801).
15. Young KC, Oduko JM, Gundogdu O, Alsager A. *Technical Evaluation of the GE Essential Full Field Digital Mammography System.* NHS Cancer Screening Programmes, 2008 (NHSBSP Equipment Report 0803).
16. Young KC, Oduko JM, Gundogdu O, Alsager A. *Technical Evaluation of the IMS Giotto Full Field Digital Mammography System with a Tungsten Tube.* NHS Cancer Screening Programmes, 2008 (NHSBSP Equipment Report 0804).
17. Young KC, Oduko JM, Gundogdu O, Alsager A. *Technical Evaluation of the Konica Minolta Regius 190 CR Mammography System and Three Types of Image Plate.* NHS Cancer Screening Programmes, 2008 (NHSBSP Equipment Report 0806).
18. Young KC, Oduko JM, Gundogdu O, Asad M. *Technical Evaluation of Profile Automatic Exposure Control Software on GE Essential Full Field Digital Mammography System.* NHS Cancer Screening Programmes, 2009 (NHSBSP Equipment Report 0903).
19. Young KC, Oduko JM, Asad M. *Technical Evaluation of the Agfa DX-M Mammography CR Reader with HM5.0 Needle-IP.* NHS Cancer Screening Programmes, 2009 (NHSBSP Equipment Report 0905).
20. Young KC, Oduko JM, Asad M. *Technical Evaluation of the Fuji Amulet Full Field Digital Mammography System.* NHS Cancer Screening Programmes, 2009 (NHSBSP Equipment Report 0907).